Dyes and Pigments 198 (2022) 110015

Contents lists available at ScienceDirect

Dyes and Pigments

journal homepage: www.elsevier.com/locate/dyepig

Red haloBODIPYs as theragnostic agents: The role of the substitution at *meso* position

Ruth Prieto-Montero [a], Alejandro Prieto-Castañeda [b], Alberto Katsumiti [c,d], Rebeca Sola-Llano [a], Antonia R. Agarrabeitia [e], Miren P. Cajaraville [c], María J. Ortiz [b], Virginia Martinez-Martinez [a,*]

[a] Departamento de Química Física, Universidad Del País Vasco/Euskal Herriko Unibertsitatea (UPV/EHU), 48080, Bilbao, Spain
[b] Departamento de Química Orgánica, Facultad de CC. Químicas, Universidad Complutense de Madrid, 28040, Madrid, Spain
[c] CBET Research Group, Department Zoology and Animal Cell Biology, Faculty of Science and Technology and Research Centre for Experimental Marine Biology and Biotechnology PiE, University of the Basque Country UPV/EHU, Basque Country, 48620, Spain
[d] GAIKER Technology Centre, Basque Research and Technology Alliance (BRTA), 48170, Zamudio, Spain
[e] Sección Departamental de Química Orgánica, Facultad de Óptica y Optometría, Universidad Complutense de Madrid, 28037, Madrid, Spain

ARTICLE INFO

Keywords:
BODIPY photosensitizer
Singlet oxygen
Photodynamic therapy
HeLa cells
Theragnosis

ABSTRACT

Three different molecular designs based on BODIPY dye have been proposed as photosensitizers (PSs) for photodynamic therapy (PDT) by the inclusion of halogen atoms (Iodine) at 2,6-positions and with extended conjugation at 3, 5-positions and varying the substitution at *meso* position. The synthesis is described and their main photophysical features including singlet oxygen production and triplet states were characterized by absorption and fluorescence spectroscopy (steady-state and time-correlated) and nanosecond transient absorption spectroscopy. The results were compared with the commercial Chlorin e6. The three new red-halogen-BODIPYs showed a great balance between singlet oxygen generation ($\Phi_{\Delta} \geq 0.40$) and fluorescence ($\Phi_{fl} \geq 0.22$) for potential application on PDT, and particularly in theragnosis. *In vitro* experiments in HeLa cells were done to study their performance and to elucidate the best potential candidate for PDT.

1. Introduction

Photodynamic therapy (PDT) is a clinically approved modality that has attracted attention as a complementary treatment to fight malignant tumors. It is a minimally invasive technique able to treat cancers after site-specific activation by light of a drug, known as photosensitizer [1–3]. The photosensitizer (PS) is activated under suitable light irradiation and generates reactive oxygen species (ROS), mainly singlet oxygen. The use of efficient photosensitizers is one of the key points to ensure the success of the PDT. The photophysical criteria to designate PDT-PS are chromophores with intense absorption bands, preferably at the therapeutic window (650–850 nm) to maximize light penetration, high singlet oxygen production and long triplet lifetimes to increase the oxidative damage and reduce the doses required and slow photobleaching rate to afford intense and long irradiation times. Moreover, PS should demonstrate suitable pharmacokinetic properties in terms of selective accumulation and excretion time from the body and negligible cytotoxicity under dark conditions to minimize side effects.

At this moment, the design and synthesis of new systems with theragnostic action, able to combine both the diagnosis and the treatment, is a very engaging strategy but usually a challenge. This has to do with the fact that although there are different approaches, imaging based on fluorescence is one of the most widely used, but fluorescent emission and singlet oxygen production are opposite photophysical features (Fig. 1). Thus, both properties should be properly balanced for a desirable fluorescent-PDT-PS [4,5].

Besides hetero tetracyclic pyrrole structures great number of non-porphyrin compounds are nowadays being synthesized and their photosensitizing ability evaluated [7–9]. One alternative compound with theragnostic properties could be BODIPY-type chromophores (Fig. 1, B). They are characterized by intense absorption bands, high fluorescence quantum yields, insensitivity to the environment and resistance to photobleaching. In spite of their high fluorescence efficiency, the BODIPY chemical structure can be easily modified in order to modulate

* Corresponding author. UNIVERSIDAD DEL PAIS VASCO. UPV-EHU Spain.
E-mail addresses: ruth.prieto@ehu.eus (R. Prieto-Montero), alprieto@ucm.es (A. Prieto-Castañeda), katsumiti@gaiker.es (A. Katsumiti), rebeca.sola@ehu.eus (R. Sola-Llano), agarrabe@quim.ucm.es (A.R. Agarrabeitia), mirenp.cajaraville@ehu.eus (M.P. Cajaraville), mjortiz@quim.ucm.es (M.J. Ortiz), virginia.martinez@ehu.eus, virginia.martinez@ehu.eus (V. Martinez-Martinez).

https://doi.org/10.1016/j.dyepig.2021.110015
Received 31 July 2021; Received in revised form 2 November 2021; Accepted 3 December 2021
Available online 4 December 2021

its final properties [10–14]. In this context, there are several strategies to enhance the population of the triplet state and consequently the singlet oxygen ($^1O_2$) production. In general, the increase of the intersystem crossing (ISC) to the triplet excited state, Fig. 1 A, is reached by incorporating heavy atoms or electron donor groups in the BODIPY skeleton [2,15–23]. Moreover, the shifting of the main BODIPY absorption band, typically located around at 500 nm, into the clinic window (>650 nm) [24], was already resolved by the replacement of carbon at the *meso* position by nitrogen, denoted as azaBODIPY [25,26], or by extending π-conjugation of the BODIPY core by several approaches [10,23,27–30]. BODIPY dye can be further functionalized by incorporating different targets [7,23,31–39], with the aim of increasing the solubility in aqueous media and enhancing the selectivity to certain organelle or malignant cells to reduce PS doses, minimize side effects, avoid drug resistance, and enhance the PDT efficacy.

Particularly in this work, the molecular design to reach red absorbing BODIPY with fluorescence and singlet oxygen production capacities is based on the following chemical modification (Fig. 2):

i) Incorporation of iodine atoms at 2,6-positions. The first example was reported by Nagano and coworkers [40]. The halo-substitution of BODIPY in those positions has been demonstrated to be the most effective for the population of the triplet states and consequently high production of singlet oxygen [15, 17,21–23,41,42]. Indeed, the increase in the number of heavy atoms attached at the BODIPY core does not necessarily increase $^1O_2$ production [18,43], as it has been previously demonstrated.
ii) Addition of styryl groups at 3,5-positions [10,44]. This approach was already revealed as a very effective to shift the absorption band to the red region in fluorescent BODIPYs. Besides, the incorporation of electron donor-groups, *i.e.* methoxy groups or dimethylamino groups in *para* position of phenyl groups, induced a larger red-shift of the absorption band [45,46].
iii) Variation of the substitution pattern at *meso* position of the BODIPY, considered as the most sensitive one due to its marked change of the electronic density upon excitation. The addition of electron donor/acceptor groups, *i.e.* nitrophenyl or aminophenyl, can modify the physico-chemical properties of BODIPY such as absorption and fluorescence emission and singlet oxygen generation [47–49] but also the lipophilicity/hydrophilicity and solubility, affecting the cell membrane permeability [30,50]. Indeed, some compounds can easily enter and diffuse into cells, *i.e.* throughout the cytosol or into particular organelles, whereas similar ones do not, which reflects the importance of the molecular design of the new PSs, and their testing into cells.

In this work, three halodistyryl BODIPY dyes, Fig. 2, were synthesized and photophysically characterized. Their main photophysical features were compared with their analog green-BODIPYs without extended conjugation at 3,5-positions (Fig. 2). *In vitro* experiments were carried out in HeLa cells to test their photoactivity and fluorescence imaging ability under regulated red light irradiation and the results were contrasted with Chlorin e6 (Fig. 2), a porphyrin-like system, which has been reported as a photodynamic drug used clinically for the treatment of lung, bladder, skin, head and neck cancer [51–54]. The phototoxicity in terms of EC_{50} was also compared with other red haloBODIPY derivatives already studied under similar conditions.

2. Materials and methods

2.1. Synthesis

2.1.1. General

Anhydrous solvents were prepared by distillation over standard drying agents according to common methods. All other solvents were of HPLC grade and were used as provided. Flash chromatography was performed using silica gel (230–400 mesh). NMR spectra were recorded using $CDCl_3$ at 20 °C. ^1H NMR and ^{13}C NMR chemical shifts (δ) were referenced to internal solvent $CDCl_3$ (δ = 7.260 and 77.04 ppm, respectively). Multiplicity is indicated as follows: s = singlet; d = doublet. Coupling constants (J) are dated in hertz (Hz). DEPT 135 experiments were used to determine the type of carbon nucleus (C *vs.* CH *vs.* CH_2 *vs.* CH_3). FTIR spectra were obtained from neat samples using the attenuated total reflection (ATR) technique. High-resolution mass spectrometry (HRMS) was performed using electronic impact (EI) or MALDI-TOF and ion trap (positive mode) for the detection.

2.1.2. Synthesis of BODIPYs

BDP-1 [40] and 8-(4-Nitrophenyl)-3,5-dimethylBODIPY [55] were synthesized by the corresponding described methods. The synthesis of the other BODIPYs is illustrated in Scheme 1.

2.1.2.1. General procedure for Knoevenagel reaction. A solution of the corresponding BODIPY (1 equiv) in DMF (3 mL), 4-methoxybenzaldehyde (3 equiv), piperidine (5 equiv) and acetic acid (5 equiv) were added to a microwave tube. The tube was sealed with an aluminum cap and heated for 20–30 min at 130 °C under microwave radiation (Biotage® Initiator Classic). After cooled down to r.t., CH_2Cl_2 was added and the organic layer was washed with water, dried over anhydrous Na_2SO_4, filtered and evaporated to dryness. The obtained residue was submitted to purification by flash chromatography on silica gel.

*2.1.2.2. Synthesis of **BDP-2**.* To a solution of 8-(4-nitrophenyl)-3,5-dimethylBODIPY [55] (50 mg, 0.14 mmol) and iodine (93 mg, 0.36 mmol) in EtOH (10 mL) was added a solution of iodic acid (51.5 mg, 0.29 mmol) in H_2O (0.5 mL), and the mixture was refluxed for 90 min. After cooling, the solvent was evaporated under vacuum. The crude product was dissolved in CH_2Cl_2, washed with a saturated solution of $Na_2S_3O_3$ and H_2O. The organic layer was dried over Na_2SO_4, filtered and concentrated to dryness. The obtained residue was purified by flash chromatography on silica gel (hexane/CH_2Cl_2, 70:30) to give **BDP-2** (74 mg, 89%) as a red solid. ^1H NMR (300 MHz, $CDCl_3$) δ 8.38 (d, J = 8.7 Hz,

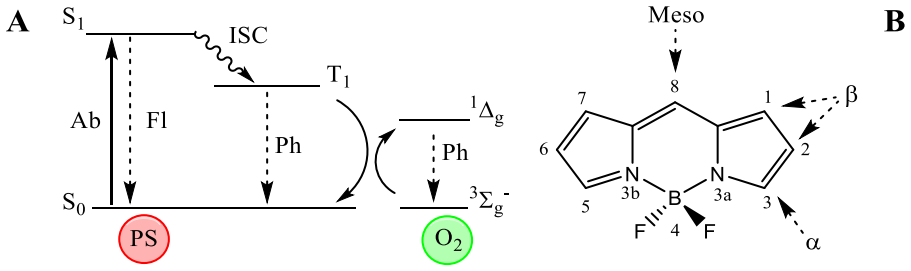

Fig. 1. (A) Jablonski diagram showing fluorescence competing with phosphorescence and ROS generation in oxygen presence. Ab: absorption, Fl: fluorescence; ISC: intersystem crossing, Ph: phosphorescence, S_0: ground singlet state, S_1: first excited singlet state; T_1: first excited triplet state, etc. (B) General BODIPY structure. The different positions are indicated and numbered according to the IUPAC system [6].

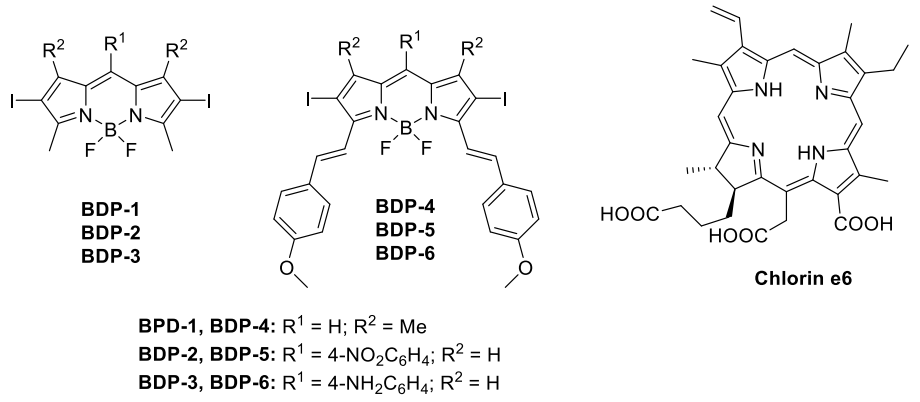

Fig. 2. Structures of new photosensitizers based on iodinated-BODIPY with different substitution patterns in *meso* in the green (**BDP-1**, **2** and **3**) and in the red (**BDP-4**, **5** and **6**) region, together with commercial porphyrin-like Chlorin e6.

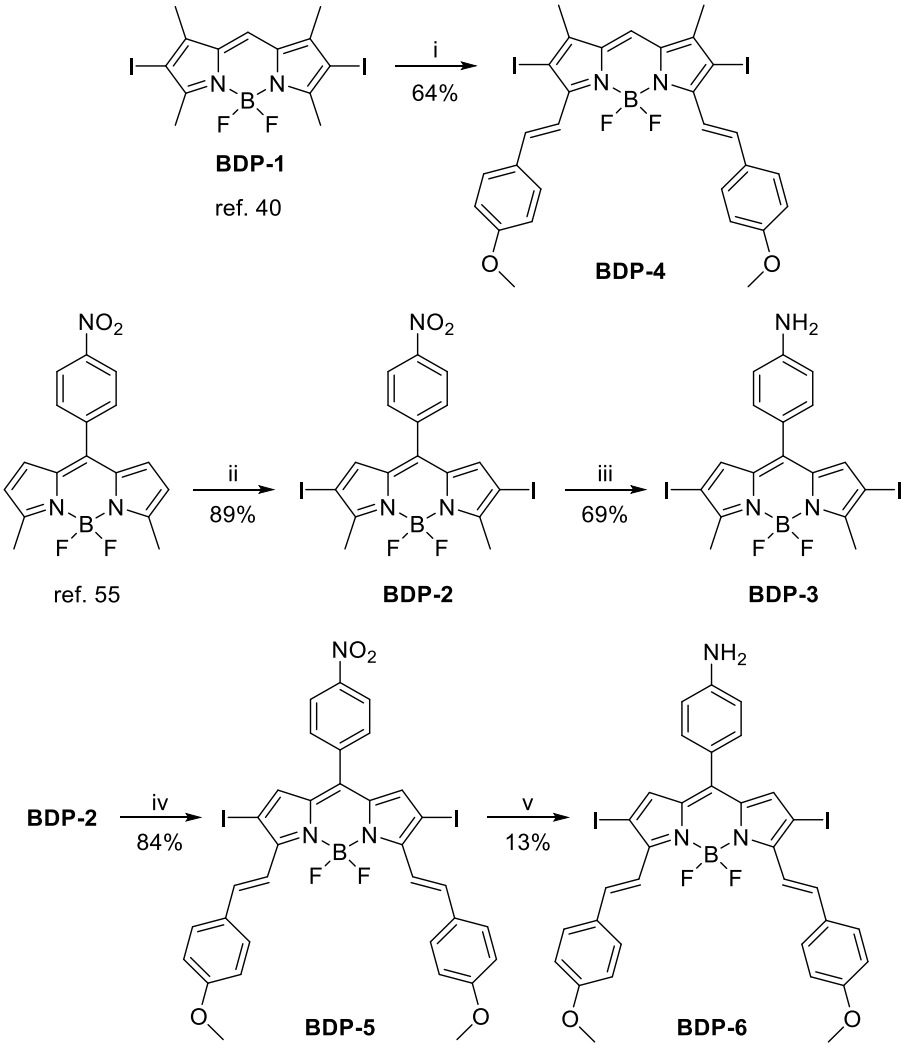

Scheme 1. Synthesis of BODIPYs. Reaction conditions: i) 4-methoxybenzaldehyde, piperidine, AcOH, DMF, 130 °C, 30 min, MW; ii) 8-(4-nitrophenyl)-3,5-dimethylBODIPY, I_2/HIO_3, EtOH/H_2O, reflux, 90 min; iii) $SnCl_2$, EtOH, reflux, 2 h; iv) 4-methoxybenzaldehyde, piperidine, AcOH, DMF, 130 °C, 20 min, MW; v) Zn powder, AcOH, rt, 90 min.

2H, 2CH), 7.66 (d, $J = 8.7$ Hz, 2H, 2CH), 6.86 (s, 2H, 2CH), 2.67 (s, 6H, $2CH_3$) ppm. ^{13}C NMR (75 MHz, $CDCl_3$) δ 160.3 (C), 149.0 (C), 139.4 (C), 137.6 (C), 136.3 (CH), 134.7 (C), 131.2 (CH), 123.8 (CH), 78.8 (C–I), 15.7 (CH_3) ppm. FTIR ν 2925, 1547, 1345, 1198, 1089, 971 cm^{-1}. HRMS-EI *m/z* 592.9120 (calcd. for $C_{17}H_{12}BF_2I_2N_3O_2$: 592.9128).

*2.1.2.3. Synthesis of **BDP-3**.* To a degassed solution of **BDP-2** (50 mg, 0.08 mmol) in EtOH (30 mL) was added $SnCl_2$ (30 mg, 0.16 mmol). The

mixture was stirred under argon atmosphere for 5 min and, past this time, was refluxed for 2 h. After cooled down to rt, the reaction was filtered and concentrated to dryness. The obtained residue was purified by flash chromatography on silica gel (CH_2Cl_2) to give **BDP-3** (31 mg, 69%) as an orange solid. ^{1}H NMR (700 MHz, $CDCl_3$) δ 7.31 (d, J = 8.4 Hz, 2H, 2CH), 7.03 (s, 2H, 2CH), 6.75 (d, J = 8.4 Hz, 2H, 2CH), 4.13 (broad s, 2H, NH_2), 2.64 (s, 6H, $2CH_3$) ppm. ^{13}C NMR (176 MHz, $CDCl_3$) δ 157.2 (C), 149.5 (C), 142.5 (C), 136.5 (CH), 134.9 (C), 132.5 (CH), 123.2 (C), 114.5 (CH), 77.4 (C–I), 15.4 (CH_3) ppm. FTIR ν 3411, 2923, 1567, 1539, 1459, 1239, 1141, 983 cm^{-1}. HRMS-EI *m/z* 562.9332 (calcd. for $C_{17}H_{14}BF_2I_2N_3$ 562.9338).

*2.1.2.4. Synthesis of **BDP-4**.* According to the general procedure, **BDP-1** [40] (170 mg, 0.34 mmol), 4-methoxybenzaldehyde (0.12 mL, 1.02 mmol), piperidine (0.17 mL, 1.70 mmol) and acetic acid (0.10 mL, 1.70 mmol) in DMF (3 mL) were reacted for 30 min at 130 °C. Flash chromatography using hexane/CH_2Cl_2 (70:30) afforded **BDP-4** (160 mg, 64%) as a red solid. ^{1}H NMR (700 MHz, $CDCl_3$) δ 8.19 (d, J = 16.8 Hz, 2H, 2CH), 7.62 (d, J = 8.4 Hz, 4H, 4CH), 7.52 (d, J = 16.8 Hz, 2H, 2CH), 7.06 (s, 1H, CH), 6.95 (d, J = 8.4 Hz, 4H, 4CH), 3.87 (s, 6H, $2CH_3O$), 2.28 (s, 6H, $2CH_3$) ppm. ^{13}C NMR (176 MHz, $CDCl_3$) δ 160.8 (C), 151.1 (C), 144.6 (C), 139.1 (CH), 134.7 (C), 129.6 (C), 129.4 (CH), 117.0 (CH), 116.6 (CH), 114.4 (CH), 79.1 (C–I), 55.5 (CH_3O), 14.3 (CH_3) ppm. FTIR ν 2956, 2922, 2853, 1580, 1510, 1465, 1248, 1210, 1148, 1086, 1010 cm^{-1}. HRMS-MALDI-TOF *m/z* 736.0061 (calcd. for $C_{29}H_{25}BF_2I_2N_2O_2$: 736.0067).

*2.1.2.5. Synthesis of **BDP-5**.* According to the general procedure, **BDP-2** (50 mg, 0.08 mmol), 4-methoxybenzaldehyde (0.03 mL, 0.25 mmol), piperidine (0.04 mL, 0.42 mmol) and acetic acid (0.02 mL, 0.42 mmol) in DMF (3 mL) were reacted for 20 min at 130 °C. Flash chromatography using hexane/CH_2Cl_2 (50:50) afforded **BDP-5** (58 mg, 84%) as a green solid. ^{1}H NMR (700 MHz, $CDCl_3$) δ 8.40 (d, J = 8.4 Hz, 2H, 2CH), 8.21 (d, J = 16.8 Hz, 2H, 2CH), 7.68 (d, J = 8.4 Hz, 2H, 2CH), 7.65 (d, J = 9.1 Hz, 4H, 4CH), 7.61 (d, J = 16.8 Hz, 2H, 2CH), 6.98 (d, J = 9.1 Hz, 4H, 4CH), 6.95 (s, 2H, 2CH), 3.88 (s, 6H, $2CH_3O$) ppm. ^{13}C NMR (176 MHz, $CDCl_3$) δ 161.3 (C), 152.7 (C), 148.8 (C), 140.2 (CH), 140.0 (C), 137.8 (CH), 136.2 (C), 133.4 (C), 131.3 (CH), 129.7 (CH), 129.3 (C), 123.8 (CH), 116.3 (CH), 114.5 (CH), 77.6 (C–I), 55.5 (CH_3O) ppm. FTIR ν 2950, 2922, 1572, 1229, 1090, 961 cm^{-1}. HRMS-MALDI-TOF *m/z* 828.9911 (calcd. for $C_{33}H_{24}BF_2I_2N_3O_4$: 828.9917).

*2.1.2.6. Synthesis of **BDP-6**.* To a solution of **BDP-5** (38 mg, 0.05 mmol) in acetic acid (2.5 mL) was added, under argon atmosphere, Zn powder (225 mg, 3.44 mmol), and the mixture was stirred to rt for 90 min. Then, the reaction was hydrolyzed with a saturated solution of $NaHCO_3$ for 20 min, diluted with EtOAc and washed with H_2O. The organic layer was dried over Na_2SO_4, filtered and concentrated to dryness. The obtained residue was purified by flash chromatography on silica gel (hexane/CH_2Cl_2/Et_3N, 60:40:0.1) to give **BDP-6** (8 mg, 13%) as a blue solid. ^{1}H NMR (700 MHz, $CDCl_3$) δ 8.11 (d, J = 16.8 Hz, 2H, 2CH), 7.62 (d, J = 8.4 Hz, 4H, 4CH), 7.59 (d, J = 16.8 Hz, 2H, 2CH), 7.32 (d, J = 8.4 Hz, 2H, 2CH), 7.14 (s, 2H, 2CH), 6.96 (d, J = 8.4 Hz, 4H, 4CH), 6.78 (d, J = 8.4 Hz, 2H, 2CH), 4.07 (broad s, 2H, NH_2), 3.87 (s, 6H, $2CH_3O$) ppm. ^{13}C NMR (176 MHz, $CDCl_3$) δ 160.8 (C), 150.9 (C), 149.1 (C), 139.0 (C), 138.5 (CH), 138.3 (CH), 136.4 (C), 132.4 (CH), 129.6 (C), 129.3 (CH), 123.6 (C), 116.7 (CH), 114.5 (CH), 114.3 (CH), 73.1 (C–I), 55.5 (CH_3O) ppm. FTIR ν 3387, 2923, 2851, 1599, 1528, 1512, 1288, 1257, 1173, 1114 cm^{-1}. HRMS-MALDI-TOF *m/z* 799.0165 (calcd. for $C_{33}H_{26}BF_2I_2N_3O_2$: 799.0175).

2.2. Photophysical characterization

The UV/Vis absorption spectra were recorded by UV–Vis–NIR Spectroscopy (Cary 7000) equipped with two lamps (halogen lamp for Vis-IR region and deuterium lamp for UV region), a double monochromator (Littrow) and double diffraction grating of 1200 lines/mm. The fluorescence and singlet oxygen measurements were recorded with an Edinburgh Instruments Spectrofluorimeter (FLSP920 model) equipped with a xenon flash lamp 450 W as the excitation source. The fluorescence spectra were corrected from the wavelength dependence on the detector sensibility. The fluorescence quantum yield (Φ_{fl}) was calculated using as reference commercial PM597 (Φ_{ref} = 0.43 in ethanol) [6] and zinc phthalocyanine (Φ_{ref} = 0.30 in 1% pyridine in toluene) [56]. The singlet oxygen quantum yields were determined by direct measurement of the luminescence at 1270 nm with a NIR detector integrated in the spectrofluorimeter (InGaAs detector, Hamamatsu G8605-23). The singlet oxygen signal was measured in the BODIPY concentration range $2{\cdot}10^{-6}$-10^{-4} M with at least five different concentrations, and the singlet oxygen quantum yield (Φ_Δ) was calculated using the following equation:

$$\Phi_\Delta^{PS} = \Phi_\Delta^{PS_{Ref}} \times \frac{S_{e,PS}}{S_{e,PS_{Ref}}} \times \frac{\alpha_{PS_{Ref}}}{\alpha_{PS}} \quad \text{Eq. 1}$$

where $\Phi_\Delta{}^{PS_{ref}}$ is the quantum yield of singlet oxygen production of the reference: 8-methylthio-2,6-diiodoBODIPY (MeSBDP, Φ_Δ = 0.91 in chloroform) [42] and New Methylene Blue (NMB, Φ_Δ = 0.50 in chloroform, characterized in the laboratory previously). The factor α = $1\text{-}10^{-A}$, being A the absorbance in the excitation wavelength, corrects the different numbers of photons absorbed by the samples and Se is the singlet oxygen signal intensity at 1276 nm. The obtained singlet oxygen quantum yields varied ±0.03–0.07 for the mean given value, being the total error always lower than 10%.

Nanosecond transient absorption measurements were recorded on a LP980 laser flash photolysis spectrometer (Edinburgh Instruments, Livingston, UK). Samples were excited by a nanosecond pulsed laser (Nd:YAG laser/OPO, LOTIS TII 2134) at the absorption maxima operating at 1 Hz and with a pulse width of 7 ns at a 3 mW excitation power. Samples with an optical absorbance of 0.3 at the excitation wavelength were deaerated with nitrogen for 10 min and aerated for 10 min with air. The triplet lifetimes that were obtained were collected on PMT detector (R928P, Hamamatsu) and oscilloscope in the presence (aerated-saturated solutions) and absence of oxygen (deaerated solution). Triplet lifetimes in the presence of oxygen (τ_T) were obtained from the slope of the recorded decay curves by means of an iterative method by LP900 software. The goodness of the exponential fit was controlled by statistical parameters (χ^2).

2.3. In vitro assays

Cell culture. Human cervix adenocarcinoma cells (HeLa cells) obtained from ATCC were grown in Dulbecco's modified Eagle's medium (DMEM) supplemented with 10% (v/v) fetal bovine serum (FBS) and 50 U/mL penicillin and 50 mg/mL streptomycin, in a humidified 5% CO_2 cell incubator at 37 °C. For the cell viability assays, cells were grown to monolayer confluency in 96-well microplates. For internalization and subcellular localization studies, cells were seeded into glass-bottom 35 mm petri dishes and subconfluent monolayers were used.

Sample preparation. The PS samples were prepared directly in DMSO (10^{-3} M) and diluted in cell culture media for *in vitro* exposures.

Internalization and subcellular localization. Cells were incubated for 24 h with 0.1, 1 and 10 μM of **BDP-4**, **BDP-5**, **BDP-6** and Ce6 PSs in 10% FBS culture medium. Unexposed cells were used as control. After incubation, cells were washed three times with culture medium, fixed with 0.4% paraformaldehyde for 10 min at 4 °C and observed under an Olympus Fluorview FV500 confocal microscope (Hamburg, Germany). Images were edited using Fiji software (ImageJ 1.49a, National Institutes of Health, Bethesda, MD, USA). The corrected total cell fluorescence (CTCF) was quantified using the Fiji software [57].

Photodynamic treatments. Cells were incubated for 24 h with 0.1, 0.5, 1, 5 and 10 μM of **BDP-4**, **BDP-5**, **BDP-6** and Ce6 PSs in 10% FBS cell

culture medium. After 24 h exposure, cells were washed three times with culture medium and maintained in the culture medium without FBS during irradiation and post-treatment time (24 h). Irradiations were performed using a light-emitting diode (LED) device (LED Par 36W from KINGBO LED) at red (λ_{max} = 655 nm), using a total light dosage of 15 Jcm^{-2}. Parallel experiments were carried out by incubating the cells with each system without irradiation to test their dark toxicity. Unexposed cells and cells exposed to 1% DMSO were used as controls. Four replicates of each treatment were used, and experiments were repeated three times.

Cell viability (MTT) assay. Light and dark cytotoxicity were assessed using the thiazolyl blue tetrazolium bromide (MTT) assay following the manufacturer's instructions. After exposures, cells were incubated with a 50 μg/mL MTT solution for 3 h at 37 °C. Then, reduced formazan product was extracted from cells with DMSO and absorbance was measured at 570 nm in a Biotek EL 312 microplate spectrophotometer reader (Winooski, USA). Cell viability was expressed as the percentage with respect to control cells. Differences between control and treated cells were analyzed through the Kruskal-Wallis test followed by Dunn's post hoc test. Differences between dark and light exposures at the same concentrations of PSs were analyzed through Mann-Whitney *U* test. EC_{50} values were calculated using the Probit test. All statistical analyses were performed using the SPSS 23.0 software (Chicago, USA). Significance level was globally established at 5% ($p < 0.05$).

3. Results and discussion

3.1. Photophysical properties

The three halodistyryl BODIPY dyes, **BDP-4**, **BDP-5** and **BDP-6**, show a bathochromic shift of their spectroscopic bands of around 150 nm [40,58–64], with respect to their analogous **BDP-1**, **BDP-2** and **BDP-3**, typically centered in the green region (Table 1, Fig. S1), locating them within the clinic window (>650 nm) [24]. The main absorption band for **BDP-4** and **BDP-6,** centered at 674 nm and 677 nm, respectively, are very close to the maxima of the red band of Chlorin e6 (Table 1, Fig. 3) [51–54]. The presence of the electron acceptor nitrophenyl group at 8 position in **BDP-5** induces a higher red shift of the absorption band, peaked at 705 m, effect previously contrasted for standard green BODIPYs [48] and in this work for halo **BDP-2**. Regarding the absorption molar coefficient in the red region, whereas **BDP-6** shows a value similar to that of Chlorin e6, the absorptivity of **BDP-4** and **BDP-5** is practically double ($\approx 8{\cdot}10^4$ $M^{-1}cm^{-1}$ *vs* $4.5{\cdot}10^4$ $M^{-1}cm^{-1}$, respectively, Table 1). An intense absorption is generally a significant parameter to reach an effective photoresponse (by the virtue of fluorescence and/or singlet oxygen generation), which maximizes the number of absorbed photons at a given PS concentration under light irradiation. In this regard, the phototoxic power (PP) and brightness (BT), defined as the product of $\varepsilon_{max}\Phi_{fl}$ and $\varepsilon_{max}\Phi_{\Delta}$, respectively (Table 1), are parameters generally applied to envisage the viability of the chromophores as fluorescent-PDT PSs. Under red light irradiation, **BDP-4** shows the lowest PP in this series, and one can expect the worst phototoxic action against cells.

Differing from the green haloBODIPYs (**BDP-1**, **BDP-2** and **BDP-3**), generally characterized by a high singlet oxygen production ($\Phi_{\Delta} \geq 0.85$) and a practically negligible fluorescence ability ($\Phi_{fl} \leq 0.07$) [30,42,63,66,67], the three red halo BODIPYs (**BDP-4**, **BDP-5** and **BDP-6**), show an attractive balance between the fluorescence efficiency and the singlet oxygen generation (Table 1), making them potential theragnostic systems to be implemented in PDT allowing optical fluorescence imaging. This fact is likely assigned to the increase of the electron delocalization in the chromophoric system by the addition of two styryl groups at 3, 5-positions, besides the expected red-shift of the absorption and emission bands, also reduces the heavy atom effect (spin orbit coupling) and consequently, the population between the singlet (fluorescence) and the triplet (singlet oxygen) states is weighted. Moreover, the fluorescence properties of these three red haloBODIPYs were characterized also in toluene and acetonitrile, Table S1. Regarding the **BDP-4**, without substitution in *meso* position, no important changes of Φ_{fl} with the polarity are detected. However, **BDP-5** and **BDP-6** undergo a fluorescence quenching in a polar solvent, *i.e.* acetonitrile, assigned to the activation of intramolecular charge transfer process favored in polar media particularly in the case of *p*-aminophenyl-BODIPY, whose decrease in the emission efficiency is more drastic.

Analyzing the changes in the photophysical properties by the different substitution pattern at *meso* position in the halodistyryl BODIPY, the incorporation of *p*-aminophenyl group, **BDP-6,** has lessened the molar absorptivity, as mentioned before, but does not produce any significant difference in the singlet oxygen quantum yield with respect to unsubstituted **BDP-4**. On the other hand, by the addition of *p*-nitrophenyl group, **BDP-5**, besides the noticeable bathochromic shift on the spectroscopic bands, an enhancement in the singlet oxygen production in the detriment of the fluorescence emission is registered when compared to **BDP-4** (Table 1).

Since the photosensitizing action always occurs via the lowest triplet state (Fig. 1), another important photophysical parameter is the triplet lifetime of PSs [68–70]. In general terms, the longer triplet lifetime is the longer interacts with the dissolved molecular oxygen and the higher oxidative damage should be expected. In order to determine if there is a relationship between these red-haloBODIPYs and their respective potential phototoxic action, the triplet lifetimes of the PSs in this series are studied.

The three BODIPYs showed similar transient absorption profiles (ns-TA) (Fig. S2): an intense negative contribution assigned to the ground

Table 1
Photophysical parameters and singlet oxygen quantum yields for iodinated-BODIPY in chloroform: absorption maxima (λ_{ab}), molar absorption coefficient (ε_{max}), fluorescence maxima (λ_{fl}), fluorescence quantum yield (Φ_{fl}), singlet oxygen quantum yield (Φ_{Δ}), brightness (BT = $\varepsilon_{max}\Phi_{fl}$) and phototoxic power (PP = $\varepsilon_{max}\Phi_{\Delta}$) at the absorption maxima wavelength.

Compounds	λ_{ab} (nm)	ε_{max} 10^4 ($M^{-1}cm^{-1}$)	λ_{fl} (nm)	Φ_{fl}	Φ_{Δ}	BT 10^4 ($M^{-1}cm^{-1}$)	PP 10^4 ($M^{-1}cm^{-1}$)
BDP-1[§] [40,65]	534	9.0	555	0.02	0.98	0.18	8.82
BDP-2	565	6.1	597	0.06[a]	0.85[c]	0.37	5.19
BDP-3	545	4.7	565	0.07[a]	0.86[c]	0.33	4.04
BDP-4	675	8.0	699	0.46[b]	0.40[d]	3.68	3.20
BDP-5	705	8.1	762	0.22[b]	0.56[d]	1.78	4.54
BDP-6	677	4.1	701	0.30[b]	0.41[d]	1.23	1.68
Chlorin e6[§]	401	13.7	669	0.16[b]	0.80[d]	2.19	10.96
	664	4.5				0.72	3.60

[§] in methanol.
[a] PM597 in ethanol Φ_{fl} = 0.43 as standard [6].
[b] Zinc phtalocyanine in 1% pyridine in toluene Φ_{fl} = 0.30 used as standard [56].
[c] MeSBDP in chloroform Φ_{Δ} = 0.91 as standard [42].
[d] NMB in chloroform Φ_{Δ} = 0.50 as standard.

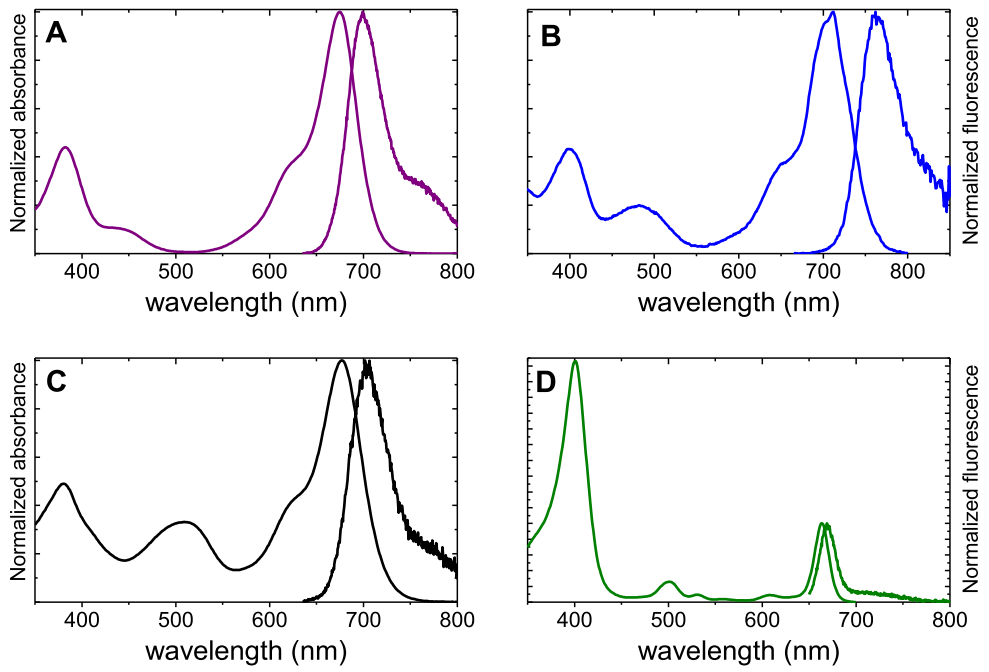

Fig. 3. Normalized absorption and emission spectra in chloroform for **BDP-4** (A), **BDP-5** (B), **BDP-6** (C) and Chlorin e6 (D).

state bleaching (GSB), in the range of 650–700 nm for **BDP-4** and **BDP-6**, and peaked at around 700 nm for **BPD-5**, associated to $S_0 \rightarrow S_1$ absorption. **BPD-4** also shows an extra and less prominent negative band at longer wavelengths with respect to GSB, assigned to the stimulated emission. All the compounds showed positive transient absorption bands in the range of 500–600 nm and at wavelengths higher than 800 nm. Decays were recorded at 550 and 850 nm in absence and presence of oxygen (Table 2 and Fig. S3). Similar lifetimes were derived at both wavelengths, indicating that it belongs to the same species. The lifetimes remained monoexponential and decreased in presence of oxygen, from 1 to 2 μs in deaerated samples to slightly lower than two hundred nanoseconds in oxygen-saturated samples (Table 2). Accordingly that, those positive transient bands are ascribed to triplet absorption. Interestingly, triplet lifetime of **BDP-6** is longer than those recorded for **BBP-4** and **BDP-5**, being the value very similar to the reported for Chlorin e6 (2 μs) [71] (Table 2). Moreover, **BDP-6** showed the highest fraction of triplet state quenched by molecular oxygen near to unity (Table 2)**.** However, **BDP-6** showed the lowest Phototoxic Power (PP in Table 1), in this series and therefore it is difficult to predict the phototoxic action of these compounds from their photophysical data. Indeed, the success of photodynamic process is controlled not only by the photophysical features but also by the internalization and selectivity degree of PSs into cells. For that, as a first approach, *in vitro* studies are required to assess their potential applicability.

Next, the most relevant results of *in vitro* experiments in HeLa cells are described and compared with those obtained for Chlorin e6 in exactly the same conditions. HeLa cells were selected for this study as they are considered as standard cell lines allowing the opportunity to contrast the current results with those derived from other studies with similar derivates and comparable light doses.

Table 2
Triplet T-T absorption maxima (λ^{T}_{max}), triplet lifetime in nitrogen- (τ^{0}), air- (τ^{air}) saturated samples, and fraction of the triplet excited state quenched by O_2 ($P^{T}_{O_2} = 1 - \frac{\tau^{air}}{\tau^{0}}$) in chloroform: **BDP-4**, **BDP-5** and **BDP-6**.

Samples	λ^{T}_{max} (nm)	τ^{0} (μs)	τ^{air} (ns)	$P^{T}_{O_2}$
BDP-4	544 840	1.07	168	0.84
BDP-5	573 880	1.25	182	0.85
BDP-6	572 860	2.26	193	0.91

3.2. *In vitro experiments with HeLa cells*

The internalization of red haloBODIPY (**BDP-4**, **BDP-5** and **BDP-6**) and Chlorin e6 in HeLa cells is shown in Fig. 4. The biocompatibility in dark conditions and the phototoxicity under red light (655 nm) irradiated for 30 min (doses = 15 J/cm^2) are shown in Fig. 5.

Based on the confocal fluorescence analysis, **BDP-4**, **BDP-6**, and Ce6 were readily incorporated by the cells whereas **BDP-5** was not internalized into the cells (Fig. 4). As seen in Fig. 4, **BDP-5** crystallized as needle-like structures at all tested concentrations, indicating a poor solubility and consequently a low cellular uptake.

On the other hand, **BDP-4**, **BDP-6** and Ce6 were internalized and homogenously accumulated throughout the cells cytoplasm. Note here that Ce6 showed a fainted brightness with respect to that recorded for **BDP-4** and **BDP-6** (Fig. 4), regardless of its BT value, which under the blue excitation condition used in the microscopy measurement was between the BT values of **BDP-4** and **BDP-6** under red light excitation (Table S2). This fact could be likely attributed to a lower internalization of Ce6 into the cells (Fig. S5). Concerning **BDP-4** and **BDP-6**, **BDP-6** showed intensity profiles/brightness 5 times higher than **BDP-4** (Fig. S5), that considering that its BT parameter at the excitation wavelength of the microscopy measurement (Table S2), is two-fold lower than that of **BDP-4**, likely indicates a higher internalization for this compound.

According to the MTT assay, none of the red haloBODIPY compounds resulted cytotoxic under dark conditions at concentrations up to 10 μM (Fig. 5 blue bars). Nonetheless, the compound **BDP-5**, with the highest PP in this series (Table 1), resulted in very low phototoxicity to HeLa cells. Actually, a relatively high amount of PS (10 μM) was required to induce only 45% of cell death under red irradiation, Fig. 5B. Indeed, as a consequence of the bad matching between the absorption spectra centered at 705 nm and the red irradiation light peaked at 660 nm, the effective PP value decreases from 3.20 10^4 $M^{-1}cm^{-1}$ (Table 1) to 1.75 10^4 $M^{-1}cm^{-1}$ (Table S2) under such red illumination source.

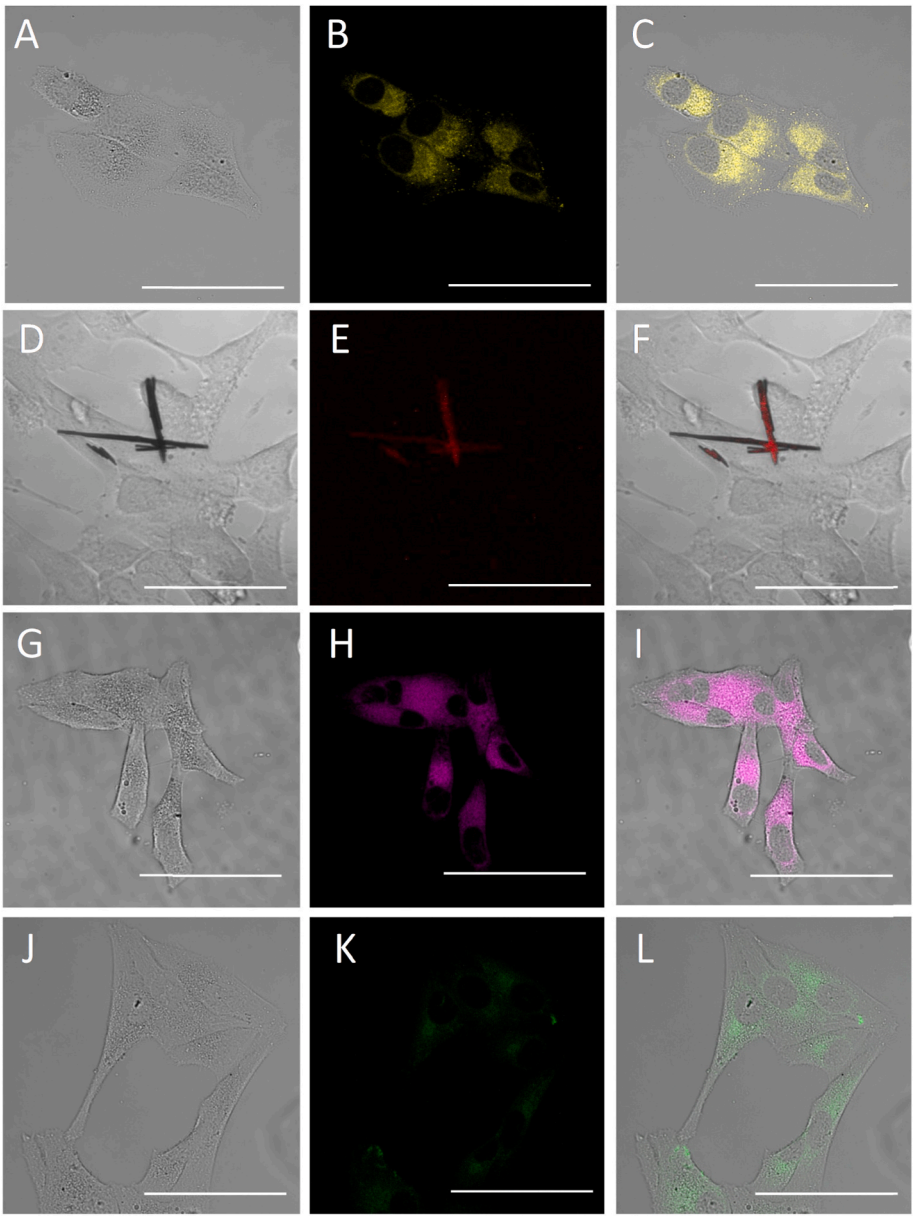

Fig. 4. Fluorescence microscopy images of compounds, **BDP-4** (A–C), **BDP-5** (D–F), **BDP-6** (G–I) (λ_{ex} = 650 nm and λ_{em} = 673 nm) and Ce6 (J–L) (λ_{ex} = 405 nm and λ_{em} = 640 nm), incubated in HeLa cells at 1 μM. The scale bars are equal to 100 μm.

Nevertheless, as the PP value under the experimental conditions of **BDP-5** is in the sample range as that of Ce6 (see data in Table S2), the mild toxicity of **BDP-5** is attributed to lack of solubility in the medium and consequently to a low internalization inside the cells [72].

On the contrary, the two red haloBODIPY-PSs (**BDP-4** and **-6**), showed high phototoxicity even at submicromolar concentrations, *i.e.* 75% and 90% of cell death was induced at 0.5 μM of **BDP-4** and **BDP-6**, respectively (Fig. 5A and C). EC_{50} values for **BDP-4** and **BDP-6** were 0.29 μM and 0.01 μM, respectively (Table 3), which are lower, particularly for **BDP-6**, than that observed for widely used commercial PS Chlorin e6 (Table 3). Although Ce6 showed a relevant photoactivity at concentrations ≥5 μM (EC_{50} = 0.67 μM, Table 3), it also caused cytotoxic effects in dark (Fig. 5D) at those concentrations, limiting its application in clinical uses. Therefore, both **BDP-4** and **BDP-6** can be enacted as promising PSs for PDT.

Note here that **BDP-6**, with the smallest effective PP at the maximum peak of the red illumination source of the series (Table S2), being practically half than those calculated for **BDP-4** and Ce6, showed the highest efficacy, leading to noticeable phototoxicity at even very low concentrations (≥0.5 μM) with EC_{50} values in the nanomolar range, 10 nM (Table 3). In the case of **BDP-6**, the high phototoxicity was probably assigned to a high cellular uptake.

Thus, the ability to be internalized into the cells is key for PDT efficacy. By simple changes in the molecular structure of the BODIPY, *i.e.* addition of an amine group (**BDP-6**), a higher solubility has been reached in comparison with its homologous BODIPY with a nitro group (**BDP-5**), increasing the internalization ability and consequently the phototoxic action. Indeed, **BDP-4** and **BDP-6**, particularly **BDP-6**, have demonstrated higher phototoxic efficiency than the commercial Chlorin e6, without showing any cytotoxic effect under dark conditions.

Other molecular designs based on the inclusion of halogen atoms (Br or I) at 2,6-positions and with extended conjugation at 3,5-positions of BODIPY dye have been proposed as PSs. Different BODIPY decoration approaches have been followed to enhance the PDT action in halodistyryl BODIPY such as pegylation, or targeting strategies to increase their solubility and cellular internalization [30,33,36,38,39,73–76].

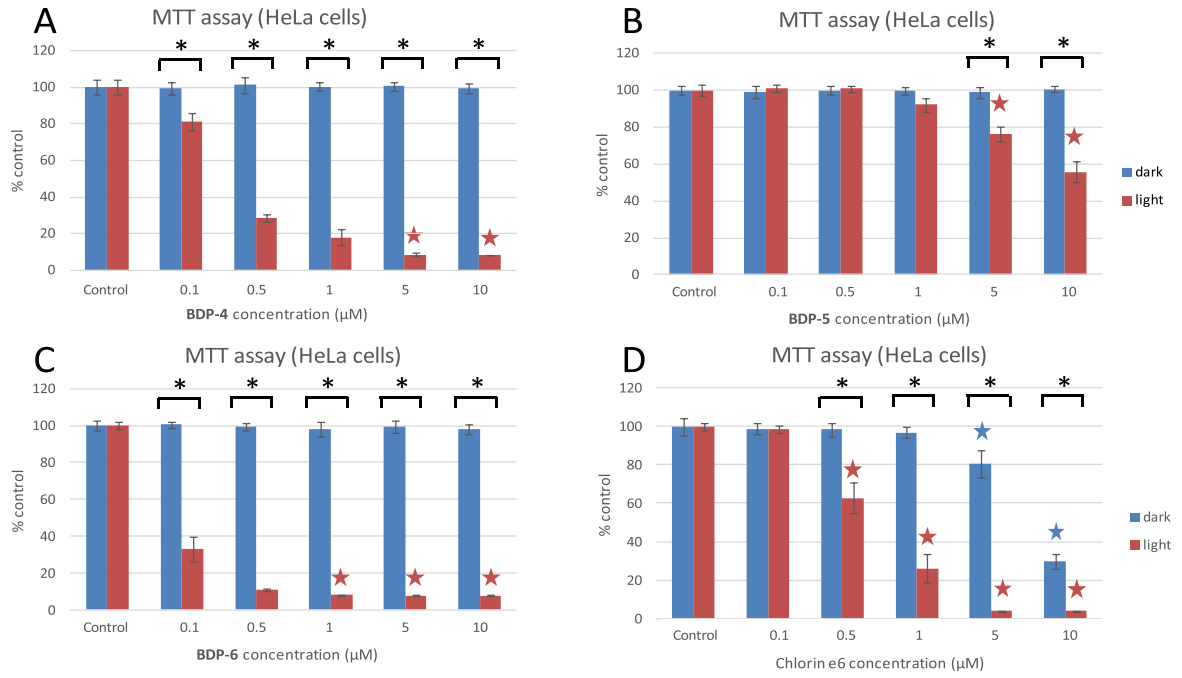

Fig. 5. MTT results of photosensitizer **BDP-4** (A), **BDP-5** (B), **BDP-6** (C) and Chlorin e6 (D) in dark conditions (blue) and after 30 min irradiation (red) under red light. Stars indicate significant differences with respect to controls. Asterisks indicate significant differences between dark and light conditions at the same concentrations tested.

Table 3
EC_{50} values of PSs under red illumination (15 J/cm^2).

	Dark (x μM)	Light (x μM)
BDP-4	–	0.29
BDP-5	–	>10
BPD-6	–	0.01
Chlorin e6	8.19	0.67

-not cytotoxic.

However, the comparison of the PDT efficiency is not trivial as there is not a standardized protocol for illumination (light dosage and light sources) and they were tested in different cell lines. To the best of our knowledge, **BDP-6** displays the highest phototoxic action against HeLa cells than any red-haloBODIPY tested so far [74,76–78].

4. Conclusion

Red iodinated-BODIPYs are promising candidates for PDT and bioimaging. They have shown intense absorption bands within the clinic window (>650 nm) and an ideal balance between fluorescence and singlet oxygen production. Nevertheless, the *in vitro* assays indicated trends that were against some of photophysical signatures, revealing the importance of the dye cell internalization. The cellular uptake was ruled by the substitution at *meso* position indicating that **BDP-5** with a *p*-nitrophenyl group at *meso* position was unable to be internalized inside the HeLa cells due to its lack of solubility in the culture medium. In contrast, **BDP-6**, homologous BODIPY but substituted with a *p*-aminophenyl at *meso*, has shown one of the highest phototoxic action against HeLa cells (EC_{50} = 10 nM) with respect to other previously developed red-haloBODIPYs tested in similar conditions, and one order of magnitude higher than the commercial Chlorin e6. In contrast to Chlorin e6, no cytotoxicity in dark conditions was found for the current red iodinated-BODIPYs.

This study demonstrates, first, the relevance of the substitution at *meso* position of BODIPYs in which simple modifications can change their performance as suitable PSs for PDT, and second, the importance of the *in vitro* assays to confirm the potential use of these molecules for bioapplications.

CRediT authorship contribution statement

Ruth Prieto-Montero: photophysical characterization Writing – original draft. **Alejandro Prieto-Castañeda:** synthesis of the compounds. **Alberto Katsumiti:** in vitro experiments. **Rebeca Sola-Llano:** photophysical characterization. **Antonia R. Agarrabeitia:** NMR studies. **Miren P. Cajaraville:** design and supervision of the in vitro experiments, financial support and review of the manuscript. **María J. Ortiz:** design and supervision of the synthesis of the compounds. **Virginia Martinez-Martinez:** design and supervision, financial support, and write the manuscript.

Declaration of competing interest

The authors declare that they have no known competing financial interests.

Acknowledgments

This research was funded by the Basque Government, grant numbers IT912-16, IT-1302-19 and IT1639-22. This work is supported by Ministerio de Ciencia, Innovación y Universidades-Agencia Estatal de Investigación (MCI/AEI), grant numbers MAT2017-83856-C3-2-P and 3-P, PID2020-114347RB-C32, PID2020-114755 GB-C32 and the University of the Basque Country (UPV/EHU), grant number COLAB19/01. R.P.M. thanks UPV/EHU for postdoctoral felowship (DOCREC 20/55). Open Access funding is provided by University of Basque Country.

Appendix A. Supplementary data

Supplementary data to this article can be found online at https://doi.org/10.1016/j.dyepig.2021.110015.

References

[1] del Rosal B, Jia B, Jaque D. Beyond phototherapy: recent advances in multifunctional fluorescent nanoparticles for light-triggered tumor theranostics. Adv Funct Mater 2018;28:1–25. https://doi.org/10.1002/adfm.201803733.

[2] Jiménez J, Prieto-Montero R, Maroto BL, Moreno F, Ortiz MJ, Oliden-Sánchez A, et al. Manipulating charge-transfer states in BODIPYs: a model strategy to rapidly develop photodynamic theragnostic agents. Chem Eur J 2020;26:601–5. https://doi.org/10.1002/chem.201904257.

[3] Li X, Kolemen S, Yoon J, Akkaya EU. Activatable photosensitizers: agents for selective photodynamic therapy. Adv Funct Mater 2017;27:1–11. https://doi.org/10.1002/adfm.201604053.

[4] DeRosa M. Photosensitized singlet oxygen and its applications. Coord Chem Rev 2002;233–234:351–71. https://doi.org/10.1016/S0010-8545(02)00034-6.

[5] Lakowicz JR. Principles of fluorescence spectroscopy. third ed. Joseph R. Lakowicz; 2006. https://doi.org/10.1007/978-0-387-46312-4.

[6] Prieto JB, Arbeloa FL, Martínez VM, López TA, Arbeloa IL. Photophysical properties of the pyrromethene 597 dye: solvent effect. J Phys Chem 2004;108:5503–8. https://doi.org/10.1021/jp0373898.

[7] Simoes JCS, Sarpaki S, Papadimitroulas P, Therrien B, Loudos G. Conjugated photosensitizers for imaging and PDT in cancer research. J Med Chem 2020;63:14119–50. https://doi.org/10.1021/acs.jmedchem.0c00047.

[8] Mfouo-Tynga IS, Dias LD, Inada NM, Kurachi C. Features of third generation photosensitizers used in anticancer photodynamic therapy: Review. Photodiagnosis Photodyn Ther 2021;34:102091–102. https://doi.org/10.1016/j.pdpdt.2020.102091.

[9] Zhao X, Liu J, Fan J, Chao H, Peng X. Recent progress in photosensitizers for overcoming the challenges of photodynamic therapy: from molecular design to application. Chem Soc Rev 2021;50:4185–219. https://doi.org/10.1039/d0cs00173b.

[10] Ziessel R, Ulrich G, Haefele A, Harriman A. An artificial light-harvesting array constructed from multiple bodipy dyes. J Am Chem Soc 2013;135:11330–44. https://doi.org/10.1021/ja4049306.

[11] Esnal I, Valois-Escamilla I, Gómez-Durán CFA, Urías-Benavides A, Betancourt-Mendiola ML, López-Arbeloa I, et al. Blue-to-orange color-tunable laser emission from tailored boron-dipyrromethene dyes. ChemPhysChem 2013;14:4134–42. https://doi.org/10.1002/cphc.201300818.

[12] Hall MJ, McDonnell SO, Killoran J, O'Shea DF. A modular synthesis of unsymmetrical tetraarylazadipyrromethenes. J Org Chem 2005;70:5571–8. https://doi.org/10.1021/jo050696k.

[13] de J, Gómez-Infante A, Bañuelos J, Valois-Escamilla I, Cruz-Cruz D, Prieto-Montero R, López-Arbeloa I, et al. Synthesis, properties, and functionalization of nonsymmetric 8-MethylthioBODIPYs. Eur J Org Chem 2016;2016:5009–23. https://doi.org/10.1002/ejoc.201600724.

[14] Rihn S, Retailleau P, Bugsaliewicz N, Nicola A De, Ziessel R. Versatile synthetic methods for the engineering of thiophene-substituted Bodipy dyes. Tetrahedron Lett 2009;50:7008–13. https://doi.org/10.1016/j.tetlet.2009.09.163.

[15] Kamkaew A, Lim SH, Lee HB, Kiew LV, Chung LY, Burgess K. BODIPY dyes in photodynamic therapy. Chem Soc Rev 2013;42:77–88. https://doi.org/10.1039/c2cs35216h.

[16] Palao-Utiel E, Montalvillo-Jiménez L, Esnal I, Prieto-Montero R, Agarrabeitia AR, García-Moreno I, et al. Controlling Vilsmeier-Haack processes in meso-methylBODIPYs: a new way to modulate finely photophysical properties in boron dipyrromethenes. Dyes Pigments 2017;141:286–98. https://doi.org/10.1016/j.dyepig.2017.02.030.

[17] Turksoy A, Yildiz D, Akkaya EU. Photosensitization and controlled photosensitization with BODIPY dyes. Coord Chem Rev 2019;379:47–64. https://doi.org/10.1016/j.ccr.2017.09.029.

[18] Prieto-Montero R, Prieto-Castañeda A, Sola-Llano R, Agarrabeitia AR, García-Fresnadillo D, López-Arbeloa I, et al. Exploring BODIPY derivatives as singlet oxygen photosensitizers for PDT. Photochem Photobiol 2020;96:458–77. https://doi.org/10.1111/php.13232.

[19] Zhang XF, Feng N. Photoinduced electron transfer-based halogen-free photosensitizers: covalent meso-aryl (phenyl, naphthyl, anthryl, and pyrenyl) as electron donors to effectively induce the formation of the excited triplet state and singlet oxygen for BODIPY compounds. Chem Asian J 2017;12:2447–56. https://doi.org/10.1002/asia.201700794.

[20] Kim B, Sui B, Yue X, Tang S, Tichy MG, Belfield KD. In vitro photodynamic studies of a BODIPY-based photosensitizer. Eur J Org Chem 2017;2017:25–8. https://doi.org/10.1002/ejoc.201601054.

[21] Gorbe M, Costero AM, Sancenón F, Martínez-Máñez R, Ballesteros-Cillero R, Ochando LE, et al. Halogen-containing BODIPY derivatives for photodynamic therapy. Dyes Pigments 2019;160:198–207. https://doi.org/10.1016/j.dyepig.2018.08.007.

[22] Killoran J, Allen L, Gallagher JF, Gallagher WM, O'Shea DF. Synthesis of BF_2 chelates of tetraarylazadipyrromethenes and evidence for their photodynamic therapeutic behaviour. Chem. Commun. 2002;317:1862–3. https://doi.org/10.1039/B204317C.

[23] Wang J, Gong Q, Wang L, Hao E, Jiao L. The main strategies for tuning BODIPY fluorophores into photosensitizers. J Porphyr Phthalocyanines 2020;24:603–35. https://doi.org/10.1142/S1088424619300234.

[24] Lacombe S, Pigot T. Materials for selective photo-oxygenation vs. photocatalysis: preparation, properties and applications in environmental and health fields. Catal Sci Technol 2016;6:1571–92. https://doi.org/10.1039/c5cy01929j.

[25] Jiang X-D, Li S, Guan J, Fang T, Liu X, Xiao L-J. Recent advances of the near-infrared fluorescent aza-BODIPY dyes. Curr Org Chem 2016;20:1736–44. https://doi.org/10.2174/1385272820666160229224354.

[26] Gorman A, Killoran J, O'Shea C, Kenna T, Gallagher WM, O'Shea DF. In vitro demonstration of the heavy-atom effect for photodynamic therapy. J Am Chem Soc 2004;126:10619–31. https://doi.org/10.1021/ja047649e.

[27] Nakamura M, Kitatsuka M, Takahashi K, Nagata T, Mori S, Kuzuhara D, et al. Yellow NIR dye: π-fused bisbenzoBODIPYs with electron-withdrawing groups. Org Biomol Chem 2014;12:1309–17. https://doi.org/10.1039/C3OB41996G.

[28] Wang DG, Zhang LN, Li Q, Yang Y, Wu Y, Fan X, et al. Dimeric BODIPYs with different linkages: a systematic investigation on structure-properties relationship. Tetrahedron 2017;73:6894–900. https://doi.org/10.1016/j.tet.2017.10.042.

[29] Lu H, MacK J, Yang Y, Shen Z. Structural modification strategies for the rational design of red/NIR region BODIPYs. Chem Soc Rev 2014;43:4778–823. https://doi.org/10.1039/c4cs00030g.

[30] Agazzi ML, Ballatore MB, Durantini AM, Durantini EN, Tomé AC. BODIPYs in antitumoral and antimicrobial photodynamic therapy: an integrating review. J Photochem Photobiol C Photochem Rev 2019;40:21–48. https://doi.org/10.1016/j.jphotochemrev.2019.04.001.

[31] Wang R, Li X, Yoon J. Organelle-Targeted photosensitizers for precision photodynamic therapy. ACS Appl Mater Interfaces 2021;13:19543–71. https://doi.org/10.1021/acsami.1c02019.

[32] Blázquez-Moraleja A, Álvarez-Fernández D, Prieto-Montero R, García-Moreno I, Martínez-Martínez V, Bañuelos J, et al. A general modular approach for the solubility tagging of BODIPY dyes. Dyes Pigments 2019;170:107545–56. https://doi.org/10.1016/j.dyepig.2019.107545.

[33] Atilgan S, Ekmekci Z, Dogan AL, Guc D, Akkaya EU. Water soluble distyryl-boradiazaindacenes as efficient photosensitizers for photodynamic therapy. Chem Commun 2006:4398–400. https://doi.org/10.1039/b612347c.

[34] Ke MR, Yeung SL, Ng DKP, Fong WP, Lo PC. Preparation and in vitro photodynamic activities of folate-conjugated distyryl boron dipyrromethene based photosensitizers. J Med Chem 2013;56:8475–83. https://doi.org/10.1021/jm4009168.

[35] Xiong H, Zhou K, Yan Y, Miller JB, Siegwart DJ. Tumor-activated water-soluble photosensitizers for near-infrared photodynamic cancer therapy. ACS Appl Mater Interfaces 2018;10:16335–43. https://doi.org/10.1021/acsami.8b04710.

[36] He H, Lo PC, Yeung SL, Fong WP, Ng DKP. Synthesis and in vitro photodynamic activities of pegylated distyryl boron dipyrromethene derivatives. J Med Chem 2011;54:3097–102. https://doi.org/10.1021/jm101637g.

[37] Zhang Q, Cai Y, Wang XJ, Xu JL, Ye Z, Wang S, et al. Targeted photodynamic killing of breast cancer cells employing heptamannosylated β-cyclodextrin-mediated nanoparticle formation of an adamantane-functionalized BODIPY photosensitizer. ACS Appl Mater Interfaces 2016;8:33405–11. https://doi.org/10.1021/acsami.6b13612.

[38] Li M, Tian R, Fan J, Du J, Long S, Peng X. A lysosome-targeted BODIPY as potential NIR photosensitizer for photodynamic therapy. Dyes Pigments 2017;147:99–105. https://doi.org/10.1016/j.dyepig.2017.07.048.

[39] Khuong Mai D, Kang B, Pegarro Vales T, Badon IW, Cho S, Lee J, et al. Synthesis and photophysical properties of tumor-targeted water-soluble BODIPY photosensitizers for photodynamic therapy. Molecules 2020;25:3340–58. https://doi.org/10.3390/molecules25153340.

[40] Yogo T, Urano Y, Ishitsuka Y, Maniwa F, Nagano T. Highly efficient and photostable photosensitizer based on BODIPY chromophore. J Am Chem Soc 2005;127:12162–3. https://doi.org/10.1021/ja0528533.

[41] Sánchez-Arroyo AJ, Palao E, Agarrabeitia AR, Ortiz MJ, García-Fresnadillo D. Towards improved halogenated BODIPY photosensitizers: clues on structural designs and heavy atom substitution patterns. Phys Chem Chem Phys 2017;19:69–72. https://doi.org/10.1039/c6cp06448e.

[42] Prieto-Montero R, Sola-Llano R, Montero R, Longarte A, Arbeloa T, López-Arbeloa I, et al. Methylthio BODIPY as a standard triplet photosensitizer for singlet oxygen production: a photophysical study. Phys Chem Chem Phys 2019;21:20403–14. https://doi.org/10.1039/C9CP03454D.

[43] Ortiz MJ, Agarrabeitia AR, Duran-Sampedro G, Bañuelos Prieto J, Arbeloa-López T, Massad WA, et al. Synthesis and functionalization of new polyhalogenated BODIPY dyes. Study of their photophysical properties and singlet oxygen generation. Tetrahedron 2012;68:1153–62. https://doi.org/10.1016/j.tet.2011.11.070.

[44] He H, Lo PC, Yeung SL, Fong WP, Ng DKP. Preparation of unsymmetrical distyryl BODIPY derivatives and effects of the styryl substituents on their in vitro photodynamic properties. Chem Commun 2011;47:4748–50. https://doi.org/10.1039/c1cc10727e.

[45] Wu W, Geng Y, Fan W, Li Z, Zhan L, Wu X, et al. BODIPY-based photosensitizers with intense visible light harvesting ability and high $^1O_2$ quantum yield in aqueous solution. RSC Adv 2014;4:51349–52. https://doi.org/10.1039/c4ra08654f.

[46] Hou Y, Liu Q, Zhao J. An exceptionally long-lived triplet state of red light-absorbing compact phenothiazine-styrylBodipy electron donor/acceptor dyads: a better alternative to the heavy atom-effect? Chem Commun 2020;56:1721–4. https://doi.org/10.1039/c9cc09058d.

[47] Bañuelos J, Martín V, Gómez-Durán CFA, Córdoba IJA, Peña-Cabrera E, García-Moreno I, et al. New 8-Amino-BODIPY derivatives: surpassing laser dyes at blue-edge wavelengths. Chem Eur J 2011;17:7261–70. https://doi.org/10.1002/chem.201003689.

[48] Li L, Nguyen B, Burgess K. Functionalization of the 4,4-difluoro-4-bora-3a,4a-diaza-s-indacene (BODIPY) core. Bioorg Med Chem Lett 2008;18:3112–6. https://doi.org/10.1016/j.bmcl.2007.10.103.

[49] Goud TV, Tutar A, Biellmann J-F. Synthesis of 8-heteroatom-substituted 4,4-difluoro-4-bora-3a,4a-diaza-s-indacene dyes (BODIPY). Tetrahedron 2006;62:5084–91. https://doi.org/10.1016/j.tet.2006.03.036.
[50] Kowada T, Maeda H, Kikuchi K. BODIPY-based probes for the fluorescence imaging of biomolecules in living cells. Chem Soc Rev 2015;44:4953–72. https://doi.org/10.1039/c5cs00030k.
[51] Fernandez JM, Bilgin MD, Grossweiner LI. Singlet oxygen generation by photodynamic agents. J Photochem Photobiol B Biol 1997;37:131–40. https://doi.org/10.1016/S1011-1344(96)07349-6.
[52] Winkler K, Simon C, Finke M, Bleses K, Birke M, Szentmáry N, et al. Photodynamic inactivation of multidrug-resistant Staphylococcus aureus by chlorin e6 and red light (λ = 670 nm). J Photochem Photobiol B Biol 2016;162:340–7. https://doi.org/10.1016/j.jphotobiol.2016.07.007.
[53] Triesscheijn M, Baas P, Schellens JHM, Stewart FA. Photodynamic therapy in oncology. Oncol 2006;11:1034–44. https://doi.org/10.1634/theoncologist.11-9-1034.
[54] Paul S, Heng PWS, Chan LW. Optimization in solvent selection for chlorin e6 in photodynamic therapy. J Fluoresc 2013;23:283–91. https://doi.org/10.1007/s10895-012-1146-x.
[55] Shin JY, Patrick BO, Dolphin D. Self-assembly via intermolecular hydrogen-bonding between o-/m-/p-NH2 and BF2 groups on dipyrromethenes. Tetrahedron Lett 2008;49:5515–8. https://doi.org/10.1016/j.tetlet.2008.07.045.
[56] Vincett PS, Voigt EM, Rieckhoff KE. Phosphorescence and fluorescence of phthalocyanines. J Chem Phys 1971;55:4131–40. https://doi.org/10.1063/1.1676714.
[57] Kim SH, Singh KB, Hahm ER, Lokeshwar BL, Singh SV. Withania somnifera root extract inhibits fatty acid synthesis in prostate cancer cells. J Tradit Complementary Med 2020;10:188–97. https://doi.org/10.1016/j.jtcme.2020.02.002.
[58] López Arbeloa F, Bañuelos J, Martínez V, Arbeloa T, López Arbeloa I. Structural, photophysical and lasing properties of pyrromethene dyes. Int Rev Phys Chem 2005;24:339–74. https://doi.org/10.1080/01442350500270551.
[59] Loudet A, Burgess K. BODIPY dyes and their derivatives: syntheses and spectroscopic properties. Chem Rev 2007;107:4891–932. https://doi.org/10.1021/cr078381n.
[60] Bessette A, Hanan GS. Design, synthesis and photophysical studies of dipyrromethene-based materials: insights into their applications in organic photovoltaic devices. Chem Soc Rev 2014;43:3342–405. https://doi.org/10.1039/c3cs60411j.
[61] Blázquez-Moraleja A, Sáenz-de-Santa María I, Chiara MD, Álvarez-Fernández D, García-Moreno I, Prieto-Montero R, et al. Shedding light on the mitochondrial matrix through a functional membrane transporter. Chem Sci 2020;11:1052–65. https://doi.org/10.1039/C9SC04852A.
[62] Lincoln R, Durantini AM, Greene LE, Martínez SR, Knox R, Becerra MC, et al. meso-Acetoxymethyl BODIPY dyes for photodynamic therapy: improved photostability of singlet oxygen photosensitizers. Photochem Photobiol Sci 2017;16:178–84. https://doi.org/10.1039/c6pp00166a.
[63] Lim SH, Thivierge C, Nowak-Sliwinska P, Han J, Van Den Bergh H, Wagnières G, et al. In vitro and in vivo photocytotoxicity of boron dipyrromethene derivatives for photodynamic therapy. J Med Chem 2010;53:2865–74. https://doi.org/10.1021/jm901823u.
[64] Boens N, Verbelen B, Ortiz MJ, Jiao L, Dehaen W. Synthesis of BODIPY dyes through postfunctionalization of the boron dipyrromethene core. Coord Chem Rev 2019;399:213024–109. https://doi.org/10.1016/j.ccr.2019.213024.
[65] Banfi S, Caruso E, Zaza S, Mancini M, Gariboldi MB, Monti E. Synthesis and photodynamic activity of a panel of BODIPY dyes. J Photochem Photobiol B Biol 2012;114:52–60. https://doi.org/10.1016/j.jphotobiol.2012.05.010.
[66] Yogo T, Urano Y, Mizushima A, Sunahara H, Inoue T, Hirose K, et al. Selective photoinactivation of protein function through environment-sensitive switching of singlet oxygen generation by photosensitizer. Proc Natl Acad Sci U S A 2008;105:28–32. https://doi.org/10.1073/pnas.0611717105.
[67] Radunz S, Wedepohl S, Röhr M, Calderón M, Tschiche HR, Resch-Genger U. PH-activatable singlet oxygen-generating boron-dipyrromethenes (BODIPYs) for photodynamic therapy and bioimaging. J Med Chem 2020;63:1699–708. https://doi.org/10.1021/acs.jmedchem.9b01873.
[68] Redmond RW, Gamlin JN. A compilation of singlet oxygen yields from biologically relevant molecules. Photochem Photobiol 1999;70:391–475. https://doi.org/10.1111/j.1751-1097.1999.tb08240.x.
[69] Dąbrowski JM, Pucelik B, Regiel-Futyra A, Brindell M, Mazuryk O, Kyzioł A, et al. Engineering of relevant photodynamic processes through structural modifications of metallotetrapyrrolic photosensitizers, 325; 2016. https://doi.org/10.1016/j.ccr.2016.06.007.
[70] Serra AC, Pineiro M, Rocha Gonsalves AMdA, Abrantes M, Laranjo M, Santos AC, et al. Halogen atom effect on photophysical and photodynamic characteristics of derivatives of 5,10,15,20-tetrakis(3-hydroxyphenyl)porphyrin. J Photochem Photobiol B Biol 2008;92:59–65. https://doi.org/10.1016/j.jphotobiol.2008.04.006.
[71] Isakau HA, Parkhats MV, Knyukshto VN, Dzhagarov BM, Petrov EP, Petrov PT. Toward understanding the high PDT efficacy of chlorin e6-polyvinylpyrrolidone formulations: photophysical and molecular aspects of photosensitizer-polymer interaction in vitro. J Photochem Photobiol B Biol 2008;92:165–74. https://doi.org/10.1016/j.jphotobiol.2008.06.004.
[72] Lin J-T. Progress of medical lasers: Fundamentals and applications. Med Dev Diagn Eng 2016;1:36–41. https://doi.org/10.15761/MDDE.1000111.
[73] Turan IS, Yildiz D, Turksoy A, Gunaydin G, Akkaya EU. A bifunctional photosensitizer for enhanced fractional photodynamic therapy: singlet oxygen generation in the presence and absence of light. Angew Chem Int Ed 2016;55:2875–8. https://doi.org/10.1002/anie.201511345.
[74] Liu J-Y, Zhou P-Z, Ma J-L, Jia X. Trifluoromethyl boron dipyrromethene derivatives as potential photosensitizers for photodynamic therapy. Molecules 2018;23:458–71. https://doi.org/10.3390/molecules23020458.
[75] Li M, Long S, Kang Y, Guo L, Wang J, Fan J, et al. De novo design of phototheranostic sensitizers based on structure-inherent targeting for enhanced cancer ablation. J Am Chem Soc 2018;140:15820–6. https://doi.org/10.1021/jacs.8b09117.
[76] Zhou Y, Cheung YK, Ma C, Zhao S, Gao D, Lo PC, et al. Endoplasmic reticulum-localized two-photon-absorbing boron dipyrromethenes as advanced photosensitizers for photodynamic therapy. J Med Chem 2018;61:3952–61. https://doi.org/10.1021/acs.jmedchem.7b01907.
[77] Padrutt R, Babu V, Klingler S, Kalt M, Schumer F, Anania MI, et al. Highly phototoxic transplatin-modified distyryl-BODIPY photosensitizers for photodynamic therapy. ChemMedChem 2020:694–701. https://doi.org/10.1002/cmdc.202000702.
[78] Tian Y, Cheng Q, Dang H, Qian H, Teng C, Xie K, et al. Amino modified iodinated BODIPY photosensitizer for highly efficient NIR imaging-guided photodynamic therapy with ultralow dose. Dyes Pigments 2021;194:109611–24. https://doi.org/10.1016/j.dyepig.2021.109611.